https://doi.org/10.46813/2025-158-107

SIMULATION OF PROPAGATION OF ELECTRON BEAMS FORMED BY HIGH-VOLTAGE GLOW DISCHARGE ELECTRON GUNS FROM LOWER TO HIGHER VACUUM

I.V. Melnyk, S.B. Tuhai, M.Y. Skrypka, O.M. Kovalenko, O.V. Bogdan
National Technical University of Ukraine “Igor Sikorsky Kyiv Polytechnic Institute”, Kyiv, Ukraine
E-mail: imelnik@phbme.kpi.ua

Based on the solution of a system of algebraic-differential equations for the boundary trajectory of an electron beam, the physical process of transporting short-focus electron beams in an ionized gas has been researched. Theoretical analysis is mainly focused on defining of the focal parameters of short-focus electron beams generated by high-voltage glow discharge electron guns. The obtained theoretical results are in good agreement with experimental data. The corresponding computer software for implementing algorithms for modeling the transportation of short-focus electron beams in ionized gas was developed using the Python program language.

PACS: 61.80.Fe, 61.82.Bg, 81.40.Wx

INTRODUCTION

Electron beam technologies are widely used in different branches of industry. Today, the use of technological electron beams extends from nanoelectronics and fine mechanics to mashing-building and metallurgy. It is caused by the high power and power density of electron beams (EB), the high efficiency of electron sources, and by the simplicity of the control of energetic and geometry parameters of electron flows in electric and magnetic fields [1 - 5].

Today, high-voltage glow discharge electron guns (HVGDEG) are widely used for providing technological operation in low and soft vacuums in the medium of active or noble gases [6 - 8]. The main advantages of HVGDEG are as follows [6 - 8]: relative simplicity of construction, wide range of operation pressure, stable operation at low and soft vacuum in the medium of different gases, and simplicity of beam power control by changing operation pressure in the discharge region [9]. For the engineering designing of such digital programming control systems, the theory of the Finite State Machine (FSM) can be successfully applied [10]. Another advantage of HVGDEG is the ability to form electronic beams with complex geometry from an enlarged cathode surface, including beams with linear and ring focusing [11].

In the present state of development, the main advantages of using HVGDEG for microelectronic production and the energetic industry are as follows.

1. Production of reliable insulation contacts for electric vehicles on the base of oxide ceramic films [12, 13].

2. Deposition of thermal-barrier coatings on turbine blades, as well as on heated parts of heat engine structures. Such advanced electron-beam technologies are also very effective today for providing novel solutions in the energy, automotive, aircraft, and space industries [12, 13].

3. Deposition of high-quality insulation ceramic films in microelectronic and nanoelectronics production, including, for example, the making of high-quality capacitors. Production by such advanced electron-beam technology of transmission and receiver devices for advanced microwave communication equipment is also possible [14].

4. Precision welding of capsules and of thin contacts in microelectronic devices, including cryogenic ones [8, 15, 16].

5. Refining of silicon as basic material for nanoelectronics production [17].

Therefore, corresponded computer software, has been elaborated for simulation the physical process of propagation of short-focus EB in the guiding channel in the medium of ionized gas is described in this paper.

In proposed model influence of magnetic field of focusing lenses, the space charge of electrons and ions, as well as dissipation of EB electrons on the ions of ionized gas are taking into account. Particularities of computer software, developed for analyzing EB propagation in the guiding channel, are also described. Obtained simulation results are compared with corresponding experimental data.

SUBJECT OF INVESTIGATIONS

Corresponding to general conceptions of high-voltage glow discharge (HVGD) physics, the operation pressure of HVGDEG should be maintained in the range of a few pascals [6 - 8]. On the contrary, much of the technological processes of EB technologies, such as the deposition of chemically complex coatings in the medium of active gases [12, 13], single-crystals growth [17], vacuum metals’ refining, etc., are realized in a smaller operation pressure range of $10^{-1}…10^{-2}$ Pa. Taking into account this fact, HVGDEG and the technological chamber have to be decoupled by pressure. The necessary difference in pressure is provided by the well-known classic method, namely, by joint pumping of an electron gun and a technological chamber with a separation gun and chamber regions by a guiding channel with a small cross-section [1 - 5]. Therefore, for the design of industrial EB equipment using HVGDEG an important scientific task is the complex research of guiding short-focus EB from the region of lower vacuum to higher in the equipotential channel.

In such circumstances, creating mathematical models for the process of guiding short-focused EB in the equipotential channel, which take into account the magnetic field of focusing lenses and the influence of residual gas, is the main aim of the researches, described in this paper. Another distinguishing feature of this model is that it takes into account the dissipation of thermal electrons' velocities. Since electrons pass through HVGD anode plasma and, after interactions with ions and dissipation, their velocity spread is range of few electronvolts [6, 7], initial thermal velocities greatly influence the geometry and energetic parameters of guiding EB. The obtained simulation results are compared with existing experimental data.

BASIC CALCULATION RELATIONSHIPS AND ASSUMPTIONS

Generally, the basic conceptions of forming such a complex model of electron-beam propagation are as follows:

1) basic principles of the optics of charged particles [1 - 5];

2) basic physical principles of discharge lighting and maintaining [18 - 20];

3) basic physical principles of vacuum technique [21, 22].

On the basis of the obtained simulation results, the conclusions about the characterized changing of EB geometry and its current in dependence on drift distance are drawn. Obtained simulation results are very important for designers of EB technological equipment.

Proposed early mathematical models for vacuum processes in the guiding pipe with rotated surface geometry characterized by such parameters as input radius R_1 and output radius R_2.

Generally, non-linear pipes, whose geometry is described by the equation:

$$r(z) = A(z+z_0)^{\alpha}, \alpha < 1, \quad (1)$$

with coefficients A and z_0, calculated through R_1 and R_2, have been considered. But the main conclusion of this study was that a slight reduction in beam current losses compared to channels of cylindrical and conical geometry does not provide the advantage of using nonlinear channels in electron beam technological equipment, taking into account the hardness of manufacturing of a channel with nonlinear shape. Therefore, only the practically used cylindrical guide system with an input diaphragm will be analyzed further in this article. A schematic diagram of a cylindrical channel for directing an electron beam with a diaphragm and one magnetic lens at the entrance to the channel is shown in Fig. 1.

Difference of pressure in electron gun and technological chamber has been provided by continuous pumping of chamber with controlled gas inlet into electron gun. Corresponded design of control system is presented in the paper [9].

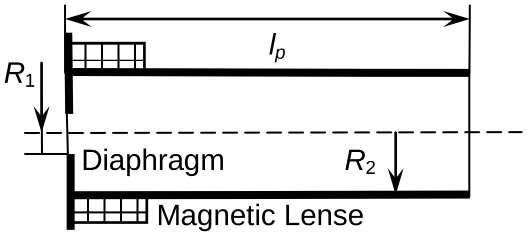

Fig. 1. The design diagram of a cylindrical channel for guiding an electron beam

The mathematical model of gas flow in the guiding channel in the general case is based on the well-known main equations of the vacuum technique and the Knudsen equation [23, 24]. For the molecular regime of gas flow resistance and conductivity of a cylindrical channel with the input diaphragm of a small cross-section, calculated as follows [21, 22]:

$$p_c = \frac{p_g U_{cyl}}{U_{cyl} + S_{p'}}; \; W_{cyl} = \frac{R_2^2 - R_1^2}{116\pi R_2^2 R_1^2} + \frac{l_p}{968 R_2^3}; \; U_{cyl} = \frac{1}{W_{cyl}}, \quad (2)$$

where p_g is pressure in the guns' chamber, p_c is pressure in the technological chamber, W_{cyl} is the vacuum resistance of guiding channel, U_{cyl} its' conductivity, l_p is length of channel, S_p is productivity of vacuum pumping.

For relatively high pressure in the discharge chamber of an electron gun, the intermediate gas flow regime in the guiding channel is usually fixed. In this case, for the calculation channel conductivity, the use of a correction coefficient J is necessary, which define as follows [21, 22]:

$$J = \frac{1 + 202(R_1+R_2)\bar{p} + 2653\left((R_1+R_2)\bar{p}\right)^2}{1 + 236(R_1+R_2)}; \; U_{im} = JU_m, \quad (3)$$

were U_m and U_{im} are the channel conductivity for molecular regime and intermediate regimes correspondently, and $\bar{p}$ is average gas pressure in channel. Values of pressure, obtained from equations (2, 3), are used later for calculation of ions' concentration in the residual gas.

Further, for calculation of the axial magnetic field of short focusing lenses, an approximation was applied, which gave suitable precision when holding true the corresponding inequality [2 - 5]:

$$0.5 \le D_l / S_l \le 2, \quad (4)$$

with wideness of nonmagnetic lens gap S_l and thickness of winding wire region D_l. The corresponding geometric parameters of a symmetric magnetic lens are given in Fig. 2 [2 - 5]. In this case, the axial magnetic field B_{z0} of a short focusing lens with ferromagnetic casing with high accuracy is defined by the following relation [2 - 5]:

$$B_{z0} = \frac{1{,}257 \cdot 10^{-4} I_l N_l}{2S_l} \left(\frac{z_l + \frac{S_l}{2}}{\sqrt{\left(\frac{D_l}{3}\right)^2 + \left(z_l + \frac{S_l}{2}\right)^2}} - \right., \quad (5)$$

$$\left. - \frac{z_l - \frac{S_l}{2}}{\sqrt{\left(\frac{D_l}{3}\right)^2 + \left(z_l - \frac{S_l}{2}\right)^2}} \right),$$

with lens current I_l, number of lens coils N_l and wideness of lens z_l.

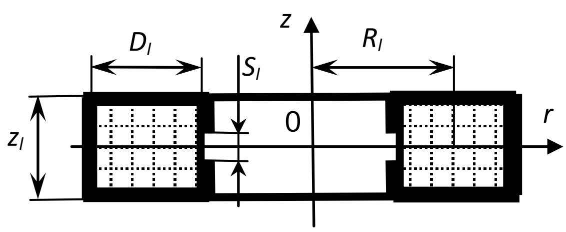

Fig. 2. Geometric parameters of magnetic lens construction

With the known axial magnetic field distribution $B_{z0}(z)$, calculated by using relations (4) and (5), the field distribution at every point of the guiding channel is obtained as a Taylor series expansion for B_r and B_z components as follows [2 - 5]:

$$B_r = -\frac{r}{2}B'_{z0} + \frac{r^3}{16}B'''_{z0} + \ldots ; \quad B_z = B_{z0} - \frac{r^2}{4}B''_{z0} + \ldots . \quad (6)$$

Calculations of the boundary EB trajectory in the guiding channel were realized in the following way. Compensation and overcompensation of beam space charge by the gas ions, pinch effect, and Rutherford scattering of electrons on the residual gas atoms are considered as physical effects that define the interaction of EB with residual gas in the guiding channel [2 - 5].

The average angle of accelerated electrons' dissipation, caused by their interaction with residual gas atoms, for the Rutherford scattering model is defined as follows [2 - 5, 7]:

$$\tan\left(\frac{\theta_{\min}}{2}\right) = \frac{10^{-4}Z_a^{4/3}}{2\gamma\beta^2};\tan\left(\frac{\theta_{\max}}{2}\right) = \frac{Z_a^{3/2}}{2\gamma\beta^2}; \quad (7)$$

$$\bar{\theta}^2 = \frac{8\pi r_b^2 n Z_a^2 z}{\beta^4\gamma^2}\ln\left(\frac{\theta_{\max}}{\theta_{\min}}\right),$$

where $\theta_{\min}$ is minimal scattering angle, $\theta_{\max}$ is maximal scattering angle, Z_a – charge of nuclear for residual gas atoms, $\beta = v/c$ is relation of electron velocity v to light velocity c, r_b is EB radius, n is concentration of gas atoms, $\bar{\theta}$ is average angle of electrons dissipation.

During simulation guiding of EB in the equipotential channel changes of slope angle for boundary beam trajectory, caused by scattering effect, namely, the average angle $\bar{\theta} = \theta_s = \frac{dr}{dz}$, calculated by using relations (7), is substituted in the equation of beam trajectory.

Influence of ions' focusing on the trajectory of beam electrons is strongly dependent on pressure and defined by ions concentration in the medium of residual gas n_{i0}, which is generally defined by the set of algebra-differential equations as follows [2 - 5, 7]:

$$n_{i0} = \sqrt{\pi} r_b^2 B_i p n_e \sqrt{\frac{M\varepsilon_0 n_e}{m_e U_c}}\exp\left(-\frac{U_c}{\varepsilon_0 n_e r_b^2}\right),$$

$$f = \frac{n_e}{n_{i0} - n_e};C = \frac{I_b\left(1 - f - \beta^2\right)}{4\pi\varepsilon_0\sqrt{\frac{2e}{m_e}}U_c^{3/2}};\frac{d^2 r_b}{dz^2} = \frac{C}{r_b} - \frac{e r_b B_{z0}^2}{8 m_e U_c}; \quad (8)$$

$$\theta = \frac{d^2 r_b}{dz^2}dz + \theta_s,$$

where B_i is the level of ionizing, p is gas pressure, n_e is concentration of electrons, m_e is mass of electron, ε_0 is dielectric constant, U_c is acceleration voltage, f is level of beam space charge compensation by ions of residual gas, I_b is beam current.

It is well-known that the spread of electrons' velocity in EB, formed by HVGDEG, is caused by its interaction with HVGD anode plasma [7]. According to early published results, after passing through anode plasma value of electron velocity spread is few electronvolts [19, 20]. For such velocity dissipation dependence of beam current density on radial coordinate r described by Gauss distribution law [2 - 5, 7]:

$$j(r) = j_0 \exp\left(-\frac{r_b^2}{\beta_b^2}\right), \quad (9)$$

where $j(r)$ is function of current density distribution, j_0 is axial current density, β_b is parameter of distribution function, characterized the dissipation of electrons velocities. In such assumption losses of beam current on the walls of guiding channel are calculated by using following equation [2 - 5, 7]:

$$dI_b = \pi\beta_b^2 j_0\left\{\exp\left[-\left(\frac{r_b - \beta_b}{2}\right)^2\right] - \exp\left[-\left(\frac{r_b}{2}\right)^2\right]\right\}, \quad (10)$$

and EB current on the number of current iteration n is simply calculated iteratively by z coordinate with taking into account its reducing, defined by equation (10):

$$I_b^n = I_b^{n-1} - dI_b^n. \quad (11)$$

With known spread of thermal electrons, the velocity parameter β_b is defined as follow. Firstly, for each part of the guiding channel, the equivalence time of electron flying is calculated by using the integral equation [2 - 5]:

$$\Delta t_e = \frac{r_b}{r_{st}}\int_{t_{st}}^{t}\left(\frac{r_{st}}{r_b}\right)^2 dt, \quad (12)$$

where r_{st} is coordinate of EB boundary trajectory on entry of guiding channel at the start time t_{st}, r_b is calculated radius of EB at current time t.

Therefore, parameter of gauss distribution β_b, which characterized the spread of electrons velocities, is defined from simple equation:

$$\beta_b = \Delta t_e\sqrt{\frac{2kT_e}{m_e}}. \quad (13)$$

Taking into account that for the physical conditions of HVGD maintaining $kT_e \approx 4$ eV [10], one can simply find coefficient β_b for current iteration by z coordinate during numerical integration of the differential equation of the boundary EB trajectory (8) with taking into account relations (7). In this calculation process, axial beam current density is defined as [2 - 5]:

$$j_0 = \frac{I_b}{2\pi\beta_b^2}. \quad (14)$$

Particularities of realizing iterative numerical calculations by the relations (2 - 14) in the elaborated computer software, created in Python program language [23 - 25], will be considered in the next section of this article. Some other approaches for the simulation of EB propagation in ionized gas, based on using statistical treatment of experimental results, have been proposed and considered in the papers [26, 27].

PARTICULARITIES OF ELABORATED COMPUTER SOFTWARE

Computer software for simulation of EB propagation in the guiding channel has been realized as a part of developed in the recent time software package, intended for the simulation, interpolation and approximation of the boundary trajectory of the short-focus EB during its propagation in ionized gas [28].

Main particularities of elaborated computer software as follows:

1. All mathematical algorithms have been realized in the level of program code using advanced approaches of functional [23 - 25] and matrix programming [29, 30].

2. For solving sophisticated simulation task and for visualization of obtained results advanced libraries of Python interpreter, such as numpy, tkinter and matplotlib have been used [23 - 25].

3. Advanced visualization graphs for scientific applications have been provided in elaborated software using the separate means of the matplotlib library [23 - 25]. These graphical objects were located among the traditional elements of user interface, such as text labels and textboxes, created with applying standard libraries of module tkinter [23 - 25].

4. To combine elements of the standard user interface and advanced scientific graphics, which are located in different libraries of the Python interpreter, in one software package, special system tools of the Windows 10 operating system were used, such as virtual variables, virtual environment, virtual memory, and virtual disk [23 - 25].

5. For simplicity of using elaborated software solving of all independent simulation tasks has been realized in the separate bookmarks. Using such approach, the exchange of data between individual tasks was implemented through the apparatus of global variables at the declarative level [28].

Corresponding bookmark for solving the task of Beam Propagation in Guiding Channel (BPGC) is presented at Fig. 3. The interface for the task of finding distributing of inductivity of the field of magnetic lenses corresponding to relations (4 - 6) is located on the separate bookmark. During simulation process changing position of lenses in the purpose of finding the minimum losses of EB current by the reason of seating the electrons on the wall of channel is possible. The number of lenses in elaborated computer software can be changed in range from 1 to 3, but, on practical point of view, using two lenses is usually enough.

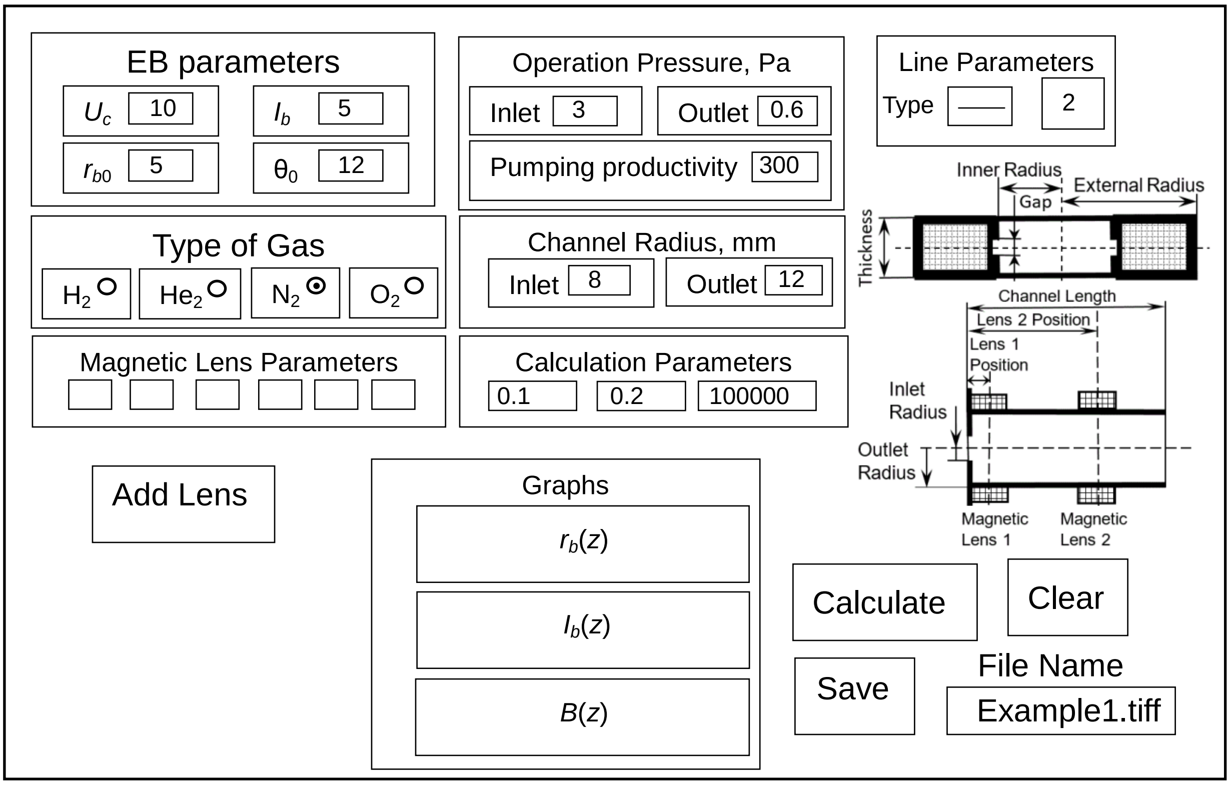

Fig. 3. Graphic interface window for simulation process of EB propagation in the guiding channel

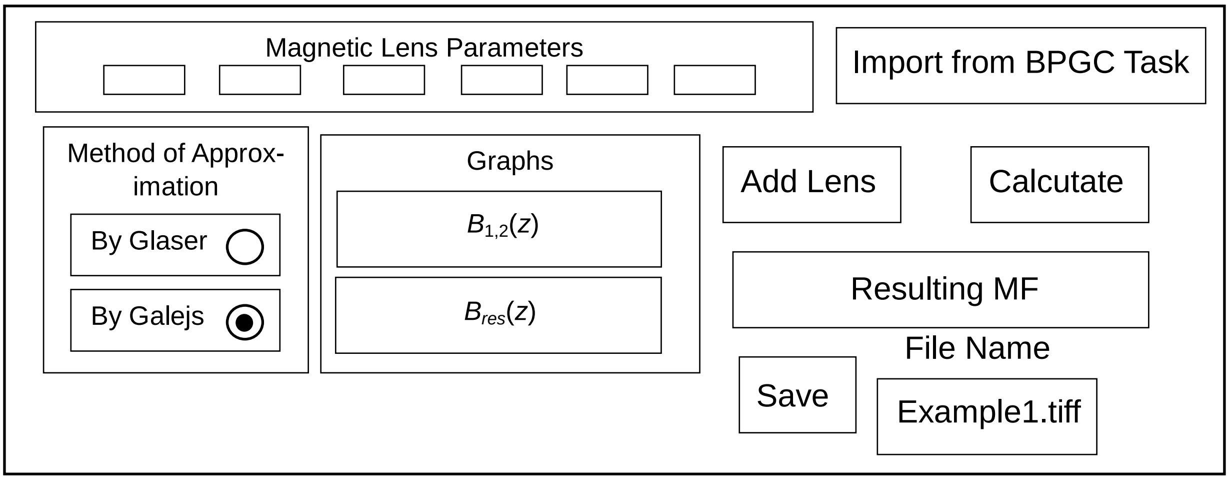

Fig. 4. Graphic interface window for simulation distribution of magnetic field of focusing lenses

ISSN 1562-6016. Problems of Atomic Science and Technology. 2025. №4(158)

Corresponding graphic interface window for visualization the result of calculation of magnetic fields distribution for two focusing lenses is presented at Fig. 4.

As it is clear from Fig. 3, the number of parameters of the simulation task of beam propagation in the guiding channel is enormous; really, it is nearly 30. Any of these parameters can be changed for visualization of the dependences of EB boundary trajectories and beam current losses on the graphs, located in the lower part of the window.

All input and output parameters of this simulation task, which are in the interface window, are classified by the physical contents corresponding to the Table 1. Restrictions imposed on the value of each input parameter are also given in this table.

Table 1

Generalized classification of input and output parameters for formulations and solutions of simulation task of beam propagation in guiding channel, corresponding to Fig. 3

Parameter		Restrictions	Task 1	Task 2
EB Input Parameters				
1	Acceleration Voltage, kV	10…40	18, 20, 22, 25	15
2	Beam Current, A	0.1…20	5	7
3	Start Beam Radius, r_b, mm	10^{-3}…50	5	8
4	Start Angle of Beam Convergence, deg.	10^{-2}…30	10	8, 10, 12, 15, 18
5	Inlet operation pressure, Pa	0.5…15	3	8
6	Outlet operation pressure, Pa	10^{-3}…1	0.6	0.4
7	Pumping productivity, m^3/s	$50…10^4$	300	150
8	Inlet channel radius R_1, mm	$r_b…10r_b$	7	10
Input Parameters of Evacuation System				
9	Outlet channel radius R_2, mm	$2r_b…20r_b$	10	15
10	Type of operation gas	Hydrogen, Helium, Nitrogen, Oxygen	Hydrogen	Oxygen
Parameters of Magnetic Lenses				
11	External Radius, mm	$2R_2…10R_2$	60, 60	60, 60
12	Inner Radius, mm	$R_2…2R_2$	10, 10	10, 10
13	Thickness, z_l, mm	$10^{-2}l_p…0.5l_p$	10, 10	10, 10
14	Gap, mm	$10^{-2}z_l…0.9z_l$	6, 4	5, 7
15	Position, m	$z_{start}+z_l/2…z_{end}-z_l/2$	0.12, 0.19	0.12, 0.165
16	Current, A	0.1…20	5, 7	5, 5.5
17	Number of Turns	$10^2…2{\cdot}10^4$	$4{\cdot}10^3$, $4{\cdot}10^3$	$4{\cdot}10^3$, $4{\cdot}10^3$
Calculation Task Parameters				
18	Start Point z Coordinate z_{start}, mm	10^{-2}…0.5	0.1	0.1
19	Last Point z Coordinate z_{end}, mm	$z_{start}+l_p$	0.2124	0.2002
20	Number of Points on z Coordinate N	$10^3…10^7$	$3{\cdot}10^5$	$3{\cdot}10^5$
21	Length of Channel, l_p, m	0.01…5	0.1124, 0.2122	0.1002
Output Parameters of Evacuation System				
22	Focus Position, m	–	0.2124, 0.2122, 0.2100, 0.2088	0.1426, 0.1431, 0.1434, 0.1439, 0.1443
EB Output Parameters				
23	EB Radius, mm	> 0	1.1379, 1.5957, 1.5533, 1.0707	0.3706, 0.3071, 0.2503, 0.1782, 0.1214
24	Current Density, kA/m^2	–	1224.84, 622.847, 657.222, 1382.48	16151.1, 23498.1, 35338.4, 69649.4, 149835
25	Power Density, MW/m^2	–	22047.2, 12451.2, 13783.2, 28928.6	2564.91, 2516.38, 2535.13, 2671.16, 2922.27
26	Summary Current Loses, mA	–	16.8053, 17.1041, 18.0437, 20.1751	55.0104, 61.4444, 68.7654, 81.6092, 97.0285

The parameters of focusing magnetic lenses are used unchangeably for calculation induction of magnetic fields, as it is clear from interface window, given in Fig. 4. But in the case, when results of this calculation don't correspond to solving simulation task, one or more of these parameters can be changed manually. Therefore, import and export of these important parameters from one to another separate simulated tasks can be realized by pressing corresponded bottoms "Import from BPGC Task" and "Export to BPGC Task", located on the top right in the interface window, presented at Fig. 4.

It is also clear from the Table 1, that with giving values of input and output operation pressure, inlet and outlet channel radii, as well as pumping productivity and type of gas, length of evacuation channel l_p is calculated automatically by relation (2), and after that this parameter is used for further simulation of guiding system and defining the EB boundary trajectories and current losses using relations (2 - 14). Corresponded value of pressure on each channel segment is defined by relation (2) and used, after that, in relations (8) for defining EB boundary trajectories. Such calculations are provided sequentially for each small channel segment, corresponding to giving number of points on z coordinate N.

Such output EB parameters, as focus position, focal beam radius, as well as focal EB current density and power density are displayed after providing calculation into corresponded textboxes, which are located on the right side of window interface (see Fig. 3).

The simulation results for the process of guiding short-focusing EB in the equipotential channel, obtained using relations (2 - 14) with elaborated computer software, are presented and discussed in the next section of this article. Corresponded input and output parameters for solving simulated tasks are also pointed out in Table 1.

SIMULATION RESULTS AND ITS' DISCUSSION

Let's consider in this section some results of solving different simulation tasks, which has been obtained using elaborating computer software.

Task 1. Finding EB boundary trajectories, as well as distribution of beam current and magnetic lenses inductivity along the channel length for the simulation task input parameters, given in the column 4 of Table 1. Define also focus position, as well as focal EB radius, current density, power density, and summary current loses.

As it clear from the data, presented at Table 1, this task has to be solved for different values of acceleration voltage: 18, 20, 22, and 25 kV. Obtained graphic dependences are given at Fig. 5.

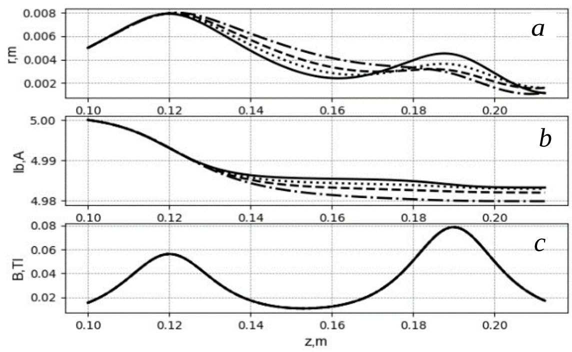

Fig. 5. Dependences of EB boundary trajectories in the guiding channel (a), current of EB (b), and distribution of focusing lenses magnetic inductivity (c) for different acceleration voltages in simulation task 1. Corresponding acceleration voltages: solid lines – 18 kV, dot – 20 kV; dash – 22 kV; dash-dot – 25 kV

In this task, two magnetic lenses have been established along the channel length in different positions of the guiding system, and corresponding input parameters of these lenses are given in column 4 of Table 1 via a comma.

It is clear from the obtained graph dependences that, generally, with increasing acceleration voltage, the focusing effect in the region of the location of the first magnetic lens is smaller, and the EB boundary trajectories are mostly lead upper. From the physical point of view, this effect is simply explained by the higher speed of the EB electrons. But, in contrast, in the region of the second magnetic lens, the focusing effect is best for the smallest acceleration voltage of 18 kV because of the higher values of the angle of EB divergence and its' radius. As a result, the relatively small value of EB radius is observed namely for the smallest acceleration voltage of 18 kV, but the smallest radius, r_b = 1.0707 mm, corresponds to the highest value of acceleration voltage, 25 kV.

As for the current losses of the EB, they are strongly increased for higher values of acceleration voltage by the reason of a greater radius of beam along the length of the guiding channel before locating the second focusing magnetic lens. All the described patterns are quite clear based on the analysis of the graphical dependencies shown in Fig. 5. The small value of the EP radius and current losses at the output of the transport system, obtained as a result of solving the simulation task at the lowest accelerating voltage of 18 kV, is primarily explained by the fact that in the simulation process the system parameters were selected as optimal namely for this value of the accelerating voltage. The output parameters of the EP after its transportation in the guide channel, obtained as a result of solving the simulation task for the specified 4 values of the accelerating voltage, are given in column 4 of Table 1, separated by commas.

Task 2. Finding EB boundary trajectories, as well as distribution of beam current and magnetic lenses inductivity for the simulation task input parameters, given in the column 5 of Table 1. Define also focus position, as well as focal beam radius, current density, power density, and summary current loses.

As it is clear from the data, presented at Table 1, this task has to be solved for different values of start angle of beam convergence: 8°, 10°, 12°, 15°, and 18°. Obtained graphic dependences are given at Fig. 6.

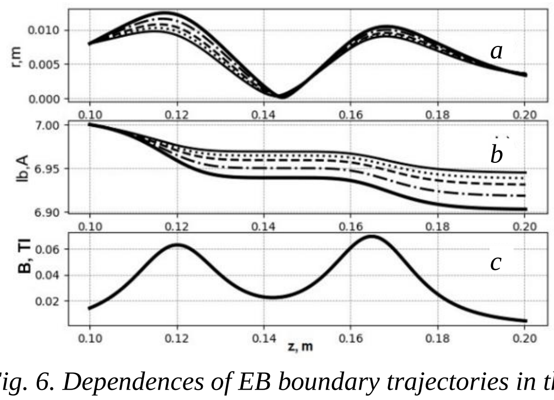

Fig. 6. Dependences of EB boundary trajectories in the guiding channel (a), current of EB (b), and distribution of focusing lenses magnetic inductivity (c) for different start angles of beam divergence in simulation task 2. Corresponding angles: thin solid lines – 8°; dot – 10°; dash – 12°; dash-dot – 15°; thick solid lines – 18°

Corresponding to dependences, presented in Fig. 6, increasing of start angle of beam convergence is, generally, lead to enlarging of radius. But the numerical data, given in the column 5 of Table 1, shown, that for higher values of the angle of beam convergence focus position is slowly removing to right and the EB radius in focus became slowly smaller. The minimum value of EB radius is r_b = 0.1214 mm and it corresponds to start angle of beam convergence α = 18°. Position of focus location for all 5 cases of simulation task is unchanged, $F \approx 0.143$ m. After point of focus the increasing of angle of EB divergence is also greater for the cases with largest start divergence angle. Therefore, almost along the entire length of the channel, the EB radius is larger for large angles of its divergence, and the beam current losses also increase in this case.

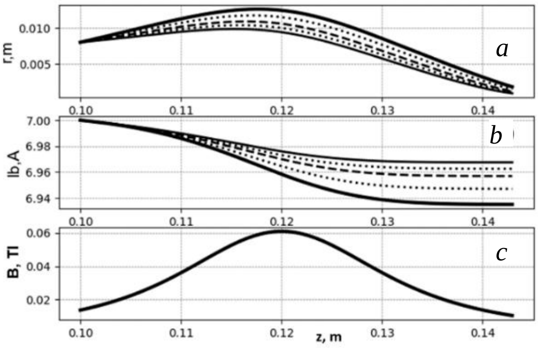

Fig. 7. Dependences of EB boundary trajectories in the guiding channel (a), current of EB (b), and distribution of only one focusing lens magnetic inductivity (c) for different start angles of beam divergence in simulation task 2. Corresponding angles: thin solid lines – 8°; dot – 10°; dash – 12°; dash-dot – 15°; thick solid lines – 18°

But it is clear also, that focusing effect of second magnetic lens is not so strong, as for first one. Therefore, output EB radius is range of 4.5 mm, and this value is significantly greater, than focal radius. In this case the best solution to improving the guiding system is reducing the length of guiding channel till the value $l_p \approx 0.1429$ m by increasing pumping productivity and excluding of second magnetic lens. In such case the EB losses also became smaller. Corresponded graph dependences for pumping productivity 350 m^3/s and $l_p = 0.1429$ m are given in Fig. 7. Output parameters of EB for such guiding system are given in Table 2.

Table 2

Output parameters of EB for Task 2 with using one focusing lens and pumping productivity 350 m^3/s

Parameter	Start angle of beam convergence				
	8°	10°	12°	15°	18°
Focal EB Radius, mm	1.5984	1.8013	2.0508	2.5007	3.03
Current Density, kA/m^2	868.35	683.360	526.78	353.846	240.4
Power Density, MW/ m^2	13025	10250.4	7901.7	5307.69	3611
Summary Current Losses, A	29.69	34.1464	39.233	48.2382	59.2

From the digital data given in Tables 1 and 2 it is clear, that in system with one magnetic lens the power density of EB is significantly greater and current losses are smaller.

Provided theoretical and experimental researches show, that for optimal conditions of beam guiding current the summary losses are smaller than 1%. Although, taking into account thermal electrons velocities, integral current losses became significantly greater, and their values are compared to experimental data. The obtained divergence of calculated and experimental data is not exceeding 15%. Measured values of beam current losses in the equipotential guiding channel for HVGDEG with different power are presented in Table 3.

Table 3

Experimental data for guiding systems for EB with different power

Beam power, kW	Acceleration voltage, kV	R_1, mm	R_2, mm	l_p, mm	Dissipated power, kW
10	12	5	7.5	150	1
50	25	7.5	10	170	3
100	30	9	15	180	6

Generally, all obtained simulation results and making conclusions are in good agreement with the basic principles of self-consistent electron-ion optics, formulated in manual books [2 - 5].

All the research results presented in this article have been obtained in the scientific laboratory of Electron-Beam Technological Devices of National Technical University of Ukraine "Igor Sikorsky Kyiv Polytechnic Institute".

CONCLUSIONS

Elaborated computer software and the simulation results that have been obtained in the provided research are very important both from a theoretical and a practical point of view. Taking into account in the model of guiding short-focused EB, formed by HVGDEG, the spread of thermal electron velocities, leads to improving of simulation accuracy and allows to estimate the real values of summary current losses. Simulation experiments have shown that the boundary trajectories of transported EB are not strongly dependent on the entry angle and that losses of beam current are mostly similar along the EB drift distance, but connected with the value of beam radius. Calculated values for integrated losses of beam current are close to real values, which have been observed experimentally. The difference between calculated and experimental data is not exceeding 15%. The results of theoretical researches, presented in the article, are very important in practice engineering activity for designers of advanced EB technological equipment on the basis of novel HVGDEGs' constructions.

The obtained simulation results may be of interest to a wide range of specialists who are involved in the physics of electron beams, their application to modern electron beam technologies, and the development of advanced EB technological equipment.

ACKNOWLEDGEMENTS

The work is financially supported by the Ministry of Education and Science of Ukraine. Priority area: new substances and materials; priority thematic area: ceramic and composite materials and coatings for extreme conditions of use; state registration number 0124U001525.

REFERENCES

1. S. Schiller, U. Heisig, S. Panzer. *Electron Beam Technology*. New-York: "John Wiley and Sons", 1982, 509 p.
2. M. Szilagyi. *Electron and Ion Optics*. Springer Science and Business Media, 2012, 539 p.
3. E. Kasper, P. Hawkes. *Principles of Electron Optics: Applied Geometrical Optics.* Elsevier Science. 1989, 1188 p.
4. P. Grivet, P.W. Hawkes, A. Septie. *Electron Optics*. Elsevier, 2013, 412 p.
5. *Electron Beams, Lenses, and Optics* / Edited by A.B. El-Kareh. Academic Press, 2012, 428 p.
6. S.V. Denbnovetsky, I.V. Melnyk, V.G. Melnyk, B.A. Tugai, S.B. Tuhai. High voltage glow discharge electron guns and its advanced application examples in electronic industry // *International Conference Radio Electronics and Info Communications (UkrMiCo)*. Kyiv, Ukraine, 2016, p. 1-4. doi: 10.1109/UkrMiCo.2016.7739615 https://ieeexplore.ieee.org/document/7739615.
7. I.V. Melnyk. Numerical Simulation of Distribution of Electric Field and Particle Trajectories in Electron Sources Based on High-Voltage Glow Discharge // *Radioelectronic and Communication Systems*. 2005, v. 48, № 6, p. 61-71.
8. I. Melnyk, S. Tuhai, M. Surzhykov, I. Shved, V. Melnyk, D. Kovalchuk. Analytical Estimation of the Deep of Seam Penetration for the Electron-Beam Welding Technologies with Application of Glow Discharge Electron Guns // *2022 IEEE 41-st International Conference on Electronics and Nanotechnology* (ELNANO). 2022, p. 1-5. doi: 10.1109/ELNANO54667.2022.9927071 https://ieeexplore.ieee.org/document/9927071.
9. S.V. Denbnovetsky, I.V. Melnyk, V.G. Melnyk, B.A. Tugai, S.B. Tuhai. Simulation of dependences of discharge current of high voltage glow discharge electron guns from parameters of electromagnetic valve // *IEEE 37th International Conference on Electronics and Nanotechnology*. 2017, p. 369-373. doi: 10.1109/ELNANO.2017.7939781 https://ieeexplore.ieee.org/document/7939781.
10. I. Melnyk, S. Tuhai, M. Surzhykov, I. Shved. Discrete Vehicle Automation Algorithm Based on the Theory of Finite State Machine. In: M. Klymash, A. Luntovskyy, M. Beshley, I. Melnyk, A. Schill. Editors // *Emerging Networking in the Digital Transformation Age*. Lecture Notes in Electrical Engineering. Springer, 2023, v. 965, p. 231-245. https://link.springer.com/chapter/10.1007/978-3-031 24963-1_13.
11. I.V. Melnyk, A.V. Pochynok. Modeling of electron sources for high voltage glow discharge forming profiled electron beams // *Radioelectronics and Communications Systems.* 2019, v. 62 (6), p. 251-261. https://link.springer.com/article/10.3103/S07352727 19060013.
12. T.O. Prikhna, I.M. Grechanyuk, M.V. Karpets, M.I. Grechanyuk, G.A. Bagliuk, V.G. Grechanyuk, V.A. Chornovol. Electron-Beam and Plasma Oxidation-Resistant and Thermal-Barrier Coatings Deposited on Turbine Blades Using Cast and Powder Ni(Co)CrALY(Si) Alloys I. Fundamentals of the Production Technology, Structure, and Phase Composition of Cast NiCrAlY Alloys // *Powder Metallurgy and Metal Ceramics*. 2022, v. 61(1-2), p. 70-76. https://www.springer.com/journal/11106.
13. T.O. Prikhna, I.M. Grechanyuk, M.V. Karpets, M.I. Grechanyuk, G.A. Bagliuk, V.G. Grechanyuk, O.V. Khomenko. Electron-Beam and Plasma Oxidation-Resistant and Thermal-Barrier Coatings Deposited on Turbine Blades Using Cast and Powder Ni(Co)CrAlY(Si) Alloys Produced by Electron-Beam Melting II. Structure and Chemical and Phase Composition of Cast CoCrAlY Alloys // *Powder Metallurgy and Metal Ceramicsthis*. 2022, v. 61(3-4), p. 230-237. https://link.springer.com/article/10.1007/s11106-022-00310-z.
14. A. Zakharov, S. Rozenko, S. Litvintsev, M. Ilchenko. Trisection Bandpass Filter with Mixed Cross-Coupling and Different Paths for Signal Propagation // *IEEE Microwave Wireless Component Letters.* 2020, v. 30, № 1, p. 12-15.
15. A.A. Druzhinin, I.P. Ostrovskii, Y.N. Khoverko, N.S. Liakh-Kaguy, A.M. Vuytsyk. Low temperature characteristics of germanium whiskers // *Functional materials*. 2014, v. 21 (2), p. 130-136.
16. A.A. Druzhinin, I.A. Bolshakova, I.P. Ostrovskii, Y.N. Khoverko, N.S. Liakh-Kaguy. Low temperature magnetoresistance of InSb whiskers // *Materials Science in Semiconductor Processing*. 2015, v. 40, p. 550-555.
17. T. Kemmotsu, T. Nagai and M. Maeda. Removal Rate of Phosphorous form Melting Silicon // *High Temperature Materials and Processes*. 2011, v. 30, № 1-2, p. 17-22. https://www.degruyter.com/journal/key/htmp/30/1-2/html.
18. B.M. Smirnov. *Theory of Gas Discharge Plasma*. Springer, 2015, 433 p.
19. M.A. Lieberman, and A.J. Lichtenberg. *Principles of Plasma Discharges for Materials Processing*. New York: "Wiley Interscience", 1994, 572 p.
20. Yu.P. Raizer. *Gas Discharge Physics.* New York: "Springer", 1991, 449 p. https://d-nb.info/910692815/04.
21. G. Lewin. *Fundamentals of Vacuum Science and Technology*. McGraw-Hill, 1965, 248 p.
22. J.M. Lafferty. *Foundations of Vacuum Science and Technology.* John Wiley & Sons, 1998, 756 p. http://vacmarket.com/assets/Technical-Library/Foundations-of-vacuum-science-and-technology/Foundations-of-vacuum-science-and-technology-1998.pdf.
23. W. McKinney. *Python for Data Analysis: Data Wrangling with Pandas, NumPy, and Jupyter /* 3rd Edition. O'Reilly Media, 2023, 579 p. https://www.oreilly.com/library/view/python-for-data/9781098104023/.
24. F. Chollet. *Deep Learning with Python* / Second Edition. Manning, 2022, 509 p.

https://www.amazon.com/Learning-Python-Second-François-Chollet/dp/1617296864/ref=zg_bs_285856_sccl_17/144-8112897-9282521?psc=1.

25. M. Lutz. *Learning Python*. Fifth Edition. O'Reilly, 2013, 1643 p.
26. V.G. Rudychev, V.T. Lazurik, Y.V. Rudychev. Influence of the electron beams incidence angles on the depth-dose distribution of the irradiated object // *Radiation Physics and Chemistry*. 2021, v. 186, p. 109527.
27. V.M. Lazurik, V.T. Lazurik, G. Popov, Z. Zimek. Two-parametric model of electron beam in computational dosimetry for radiation processing // *Radiation Physics and Chemistry*. 2016, v. 124, p. 230-234. https://www.oreilly.com/library/view/learning-python-5th/9781449355722/.
28. I. Melnyk, S. Tuhai, M. Skrypka, T. Khyzhniak, A. Pochynok. *A New Approach to Interpolation and Approximation of Boundary Trajectories of Electron Beams for Realizing Cloud Computing Using Root-Polynomial Functions* / S. Dovgyi, O. Trofymchuk, V. Ustimenko, L. Globa. Editors. Information and Communication Technologies and Sustainable Development. ICT&SD 2022. Lecture Notes in Networks and Systems. Springer, 2023, v. 809, p. 395-427. ISBN 978-3-031-46879-7. Cham. https://doi.org/10.1007/978-3-031-46880-3_24
29. I. Melnyk, A. Luntovskyy. *Estimation of Energy Efficiency and Quality of Service in Cloud Realizations of Parallel Computing Algorithms for IBN*. Future Intent-Based Networking. On the QoS Robust and Energy Efficient Heterogeneous Software Defined Networks / M. Klymash, M. Beshley, A. Luntovskyy Editors. Lecture Notes in Electrical Engineering, 831. Chapter 20. Springer, 2022, p. 339-379. ISBN 978-3-030-92433-1. https://link.springer.com/chapter/10.1007/978-3-030-92435-5_20.
30. J.H. Mathews, K.D. Fink. *Numerical Methods*. Using Matlab. Third Edition. Amazon, 1998, 720 p.

Article received 11.03.2025

МОДЕЛЮВАННЯ ПОШИРЕННЯ ЕЛЕКТРОННИХ ПУЧКІВ, СФОРМОВАНИХ ЕЛЕКТРОННИМИ ГАРМАТАМИ ВИСОКОВОЛЬТНОГО ТЛІЮЧОГО РОЗРЯДУ, З НИЗЬКОГО ДО ВИСОКОГО ВАКУУМУ

І.В. Мельник, С.Б. Тугай, М.Ю. Скрипка, О.М. Коваленко, О.В. Богдан

На основі вирішення системи алгебродиференціальних рівнянь для граничної траєкторії електронного пучка досліджено фізичний процес транспортування короткофокусних електронних пучків у іонізованому газі. Теоретичний аналіз, головно, зосереджено на визначенні фокальних параметрів короткофокусних електронних пучків, що генеруються електронними гарматами високовольтного тліючого розряду. Отримані теоретичні результати добре узгоджуються з експериментальними даними. На мові програмування Python розроблено відповідне комп’ютерне програмне забезпечення для реалізації алгоритмів моделювання транспортування короткофокусних пучків електронів у іонізованому газі.